Michael Stöhr, Stephan Ruoff, Bastian Rauch, Wolfgang Meier and Patrick Le Clercq, Droplet vaporization for conventional and alternative jet fuels at realistic temperature conditions: Systematic measurements and numerical modeling, Proceedings of the Combustion Institute 38 (2021) 3269–3276.

The original publication is available at www.elsevier.com

https://doi.org/10.1016/j.proci.2020.05.015

Droplet vaporization for conventional and alternative jet fuels at realistic temperature conditions: systematic measurements and numerical modeling

Michael Stöhr[a,*], Stephan Ruoff[a], Bastian Rauch[a], Wolfgang Meier[a], Patrick Le Clercq[a]

[a]*German Aerospace Center (DLR), Institute of Combustion Technology, Pfaffenwaldring 38-40, 70569 Stuttgart, Germany*

Abstract

The desired reduction of fossil fuel consumption of the aviation sector requires the introduction of alternative jet fuels from renewable sources. A major hurdle for their introduction is the cost-intensive assessment of fuel effects on combustion performance, which relies on fuel-dependent processes such as atomization, vaporization and chemical reaction. The present work describes results from a newly designed experiment that provides accurate measurements of vaporization of free-falling droplets of realistic size (D≈80 μm) in a vertical laminar flow with temperatures typical of technical combustors. Measurements are performed for a set of systematically chosen conventional and alternative multi-component jet fuels for which detailed compositions are available, and for three single species. The results show that the differences of their vaporization can be accurately resolved and related to physical properties. In particular, it is found that the effect of fuel boiling point on vaporization is largest for ambient gas temperatures T_∞ below ≈1000 K, whereas for higher T_∞ the influence of heat of vaporization is dominant. The well-defined boundary conditions of the experiment further enable a numerical simulation of the ambient flow and the droplet vaporization, where the latter uses a multi-component vaporization model based on a continuous thermodynamic representation of chemical species. Comparisons to measurements show that the present model accurately predicts the temporal evolution of droplet diameters and fuel-dependent effects on vaporization.

Keywords:
Alternative jet fuels, Droplet vaporization, Validation experiment, Multi-component vaporization modeling

1. Introduction

The adverse effects on atmosphere and climate, the foreseeable decline in petroleum reserves and the expected major growth of air transportation have induced a strong demand for reduction of fossil fuel comsumption of the aviation sector [1–3]. Besides improvements of propulsion efficiency, the introduction of alternative jet fuels (AJFs) from renewable sources is the central element of the related efforts [2, 3]. Until 2018, five types of synthesized blending components for conventional jet fuel (CJF) have been approved within the standard specification ASTM D7566 [4]. The extensive testing requirements for approval, however, currently restrict the introduction of additional AJFs. Governments and industry in EU and USA have therefore initiated the research programmes JETSCREEN [5] and NJFCP [6], respectively, which aim at identifying methods for efficient prescreening and optimization of promising AJF candidates. Especially for the combustion testing part, numerical simulation can be beneficially used to reduce costs and time.

The safety and emissions of aero-engines largely depend on a stable and clean operation of the combustor. Various critical issues such as altitude relight, lean blowout and soot formation are goverened by a number of complex and mutually interacting subprocesses including fuel atomization, vaporization, turbulent mixing and chemical reaction [7–9]. The subprocesses in turn depend on various physical and chemical properties of the fuels. Finding accurate relations between the fuel properties and the combustion performance is one of the major challenges for the approval of novel AJFs.

The present work adresses the process of fuel vaporization. While for single-component fuels suitable models are available [10], accurate and efficient modeling for jet fuels is still under development, mainly

*Corresponding author:
Email address: michael.stoehr@dlr.de (Michael Stöhr)

due to diffculties arising from their composition of typically hundreds of chemical species. The broad range of species can lead to differential vaporization of light- and heavy-end components, which causes variations of the chemical composition of the vapor throughout the flame zone. Recent engine tests by Won et al. showed that this effect can impact the lean blowout limit of combustors [9]. A LES of an aero-engine combustor by Eckel et al. lately further highlighted possible effects of differential vaporization on soot formation [11]. A recent numerical simulation by Stagni et al. also revealed the role of preferential vaporization on the ignition of a homogeneous spray/air mixture [12]. It is thus concluded that accurate calculation of multi-component vaporization at applicable computational cost is an important requisite for modeling combustors operated with CJFs or AJFs.

The development of models for multi-component vaporization is currently an active field of research. The main modeling classes include continuous thermodynamic models (CTM) [13–16], distillation-curve methods [17], discrete-component methods [18] and quasi-discrete models [19]. The former two methods approximate the multi-component mixture as one or several continuous distribution functions, which allows for a computationally efficient implementation. The (quasi-)discrete models provide a more detailed representation that, however, becomes computationally impractical for large number of components, and requires accurate physical properties for numerous rare species which are difficult to obtain [20].

A major hindrance for assessment and improvement of these models is the limited availability of validation data. The data for testing the above models [21–24] was limited to a small number of fuels with often unknown composition. Also droplets were mostly measured at temperatures significantly below those in technical combustors with sizes often much larger than those in real engines (D<100 μm), and in some cases undesired influences from suspension fibers arise. The notable work of Wilms [25] was limited to 350 K and maximal 3 components. Other experiments with more realistic conditions were focusing on droplet ignition [26] or restricted to few single-component fuels [27].

The current study aims at providing accurate validation data for a set of aviation-relevant fuels whose composition is well-specified and that are measured under well-defined boundary conditions. We present a newly designed experiment where droplets of realistic size (D≈80 μm) are injected into a laminar flow of exhaust gas with temperatures up to 1300 K. Microscopic shadowgraphy provides precise measurements of droplet diameters over time. Tested fuels comprise 3 CJFs, 3 already approved AJFs and 3 pure n-alkanes. The results are used to discuss effects of distillation curve and heat of vaporization. Furthermore, a numerical simulation of the gaseous flow and multi-component vaporization using CTM is tested against the measurements.

2. Methods

2.1. Experimental setup

The vaporization of fuel droplets is measured in a vertical channel sketched in Fig. 1. A flow of premixed methane and air (27.3 g/min, equiv. ratio ϕ=1) is introduced into a plenum and then passes through a water-cooled, porous bronze matrix. Methane and air react in a flat flame attached to the downstream surface of the matrix, and the burned gas then flows downward in a vertical channel of 60×60 mm^2 cross-section. The 4 sidewalls are made of quartz glass in order to provide optical access for shadowgraphy. Single droplets of D=77±1 μm are generated by a piezo-driven dispenser head (Microdrop MD-K-140) above the plenum and are injected into a vertical steel tube (d=5 mm) whose exit is located 5 mm below the bronze matrix. A nitrogen purge flow of 0.5 g/min and T≈30°C is applied in the vertical tube for rapid transport of droplets into the hot gas. Mass flow rates of methane, air and nitrogen were measured using Coriolis flow meters with an uncertainty of 2%.

In both the tube and the channel the flow is laminar with centerline velocities in the range of 0.8 to 1 m/s. Flat-flame exhaust gas temperatures for the same matrix type have been measured by Weigand et al. [28] for various flow rates and values of ϕ, and from this a value of T=1891 K is obtained for the present conditions. Therefore, well-defined boundary conditions in terms of velocity, temperature and composition (using GasEq [29]) are available for the droplet vaporization domain (cf. Sect. 2.2). The droplets are injected periodically with a maximum frequency of 40 Hz, which ensures that the distance between droplets is larger than 200 diameters and thus no inter-droplet interaction occurs.

The evolution of droplet diameter and velocity as a function of the distance x from the tube exit is measured using microscopic double-pulse shadowgraphy. The laser pulses from a dual-cavity Nd:YAG-Laser (λ=532 nm, E=2×80 mJ, Δt=50μs) are widened to d=100 mm using a concave lens and directed onto a fluorescent screen that provides the desired non-coherent illumination. Resulting double-images of the droplet shadow are recorded using a long-distance microscope (Questar

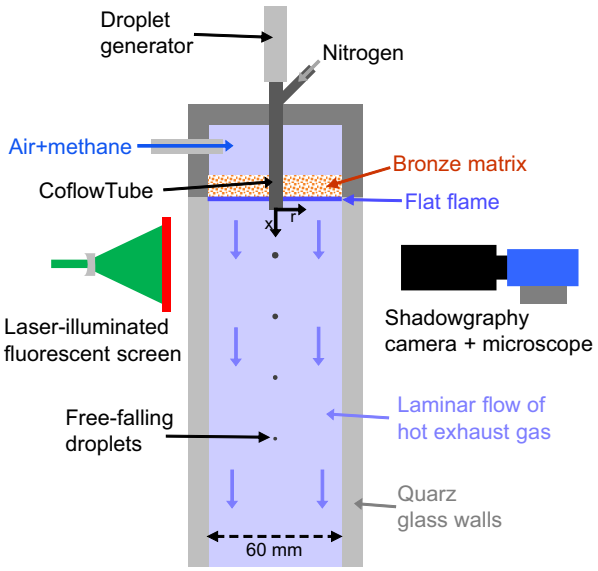

Figure 1: Schematic setup of droplet flow channel and shadowgraphy.

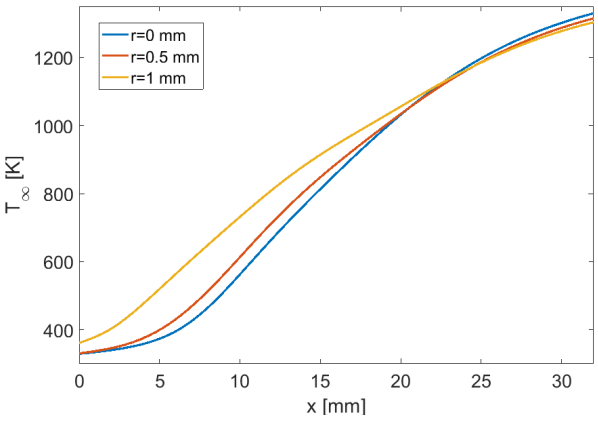

Figure 2: Axial profiles of ambient gas temperature $T_\infty(x)$ for r=0, 0.5 and 1 mm obtained from numerical simulation.

QM100) mounted on a CCD camera (Lavision Imager intense). An in-house image processing code calculates the droplet size $D(x)$ and axial velocity $v(x)$ from the image pairs. 200 measurements each are made at positions starting from x=1 mm and increasing in steps of Δx=1 mm until the droplet disappears. At each position, the RMS deviations of measured D and v are within ±1 μm and ±0.02 m/s, respectively. For the variation of x, the channel is moved vertically using a translation stage while the optical setup remains fixed. The delay of the trigger signals for laser and camera relative to the timing of droplet generation is adapted for each position x such that the droplets appear in the field of view. The according times $t(x)$ are calculated using the measured $v(x)$ as $t(x) = \int_{1\mathrm{mm}}^{x} 1/v \, \mathrm{d}x'$.

The major part of measurement uncertainties is caused by five effects: (a) variation of ambient temperatures due to slight radial displacement of droplet trajectories (cf. Sect. 2.2), (b) variation of initial droplet diameter of D_0=77±1 μm, (c) variation of ambient pressure p_a=1000±30 mbar causing changes of flow velocities of about ±3% at the given fixed mass flow rates, (d) the uncertainties of mass flow meters specified above, and (e) the uncertainty of droplet diameter measurement as noted above. In order to estimate the overall uncertainties including variations from all effects, repeated measurements were performed for several of the reported cases. The x-dependent uncertainties of D and K shown in Figs. 4 and 5 were then determined as the deviations between the respective repeated measurements.

2.2. *Numerical modeling*

The gaseous flow in the channel is computed by the DLR in-house code THETA [30] that employs a 3D finite-volume solver for unstructured grids. The underlying equations are the conservation of mass, momentum, species (N_2, O_2, H_2O, CO_2, CO, OH) and enthalpy. The model also includes buoyancy-effects and convection-diffusion equations for heat and species. Radiative heat loss from the two dominant gaseous species CO_2 and H_2O is included using a heat sink approach in an optically thin medium [31]. The flows into the channel and tube are defined by the mass flow, temperature and chemical composition specified in Sect. 2.1. The matrix flame is modeled as a source of hot exhaust gas where no further reactions occur. The lateral boundaries are represented by isothermal walls and a fixed pressure is applied at the outlet.

The resulting axial profiles of gas temperature T_∞ are plotted in Fig. 2 for the channel centerline (r=0 mm) and radial positions of r=0.5 and 1 mm. The profile for r=0 mm shows that T_∞ remains below 400 K until x=6 mm, and then continuously increases due to radial mixing with the hot exhaust gas surrounding the nitrogen purge flow. It is also seen that at slightly increased radial positions such as r=0.5 and 1 mm, the values of T_∞ are considerably higher. During the experiments it was therefore taken care that radial positions of droplets are within $r \leq 0.2$ mm in order to ensure similar conditions for all fuels.

The droplet behavior is computed by the DLR in-house Lagrangian particle tracking code SPRAYSIM, which solves the coupled ordinary differential equations

for position, velocity, diameter, temperature and composition as described in Ref. [32]. The computation of transient droplet vaporization is based on the model of Abramzon and Sirignano [10] with slightly modified terms for Reynolds-dependence [32]. For multi-component fuels, the model employs the CTM approach described by Le Clercq et al. [15] together with a rapid-mixing assumption (RMA). The CTM approximates the large number of species in complex fuel mixtures by a description via distribution functions (for details see Ref. [11]). For the NJFCP fuels (see Sect. 3) the composition is described by five distribution functions representing the fuel families of n-alkanes, iso-alkanes, cyclo-alkanes, mono- and di-aromatics, respectively. The droplet modeling starts at x=1 mm and uses the measured velocity and diameter at this position as starting condition.

3. Fuels

A set of 9 fuels in 3 groups was selected that provides a systematic and broad variation of physical properties in order to analyze their effects on the vaporization characteristics. For all multi-component fuels the exact composition is available in the supplemental material, which is important for model testing. The main properties and distillation curves are given in Table 1 and Fig. 3, respectively. The first group includes the CJFs Jet A (POSF 10325), JP-5 (POSF 10289) and JP-8 (POSF 10264) provided by the US NJFCP [6]. These fuels cover the range of properties seen in current petroleum-derived jet fuels, and are specified in detail in Ref. [33]. All three are relatively wide-boiling fuels with notable shifts of T_{50} from 190°C for JP-8 to 220°C for JP-5 and aromatic contents between 11.2 and 18 Vol.%.

The 3 chosen AJFs, namely HEFA, AtJ and Farnesane, are all approved and annexed in ASTM 7566, and have already been operated in commercial passenger flights with blending ratios between 10% and 50% [3]. HEFA has a similar T_{50} as Jet A, but a notably lower T_0 and thus contains more volatile light-end components. AtJ exhibits a rather unusual boiling curve including a very narrow distillate around 180°C up to 80 Vol% together with a small high-boiling fraction ranging up to 259°C. Farnesane is a pure C_{15} iso-alkane with a boiling point of 247°C. All 3 AJFs are virtually free of aromatics.

Finally 3 single-component (SC) fuels, namely n-nonane, n-dodecane and n-pentadecane, were studied in order to enable tests of vaporization models without extension for multiple components. Fig. 3 shows that their respective boiling points lie at the bottom, middle and top of the range covered by the multi-component fuels.

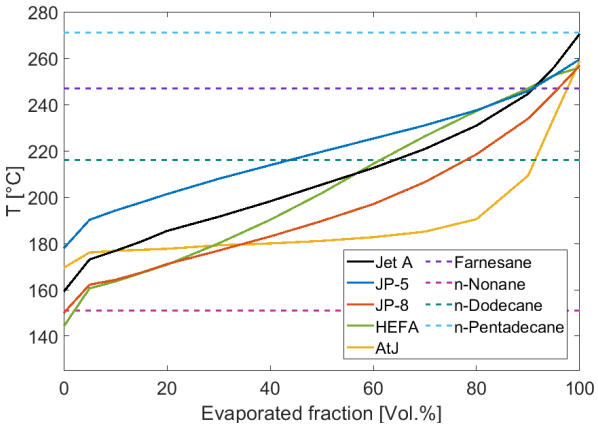

Figure 3: Distillation curves of multi-component fuels (solid lines) and boiling points of single-component fuels (dashed lines).

4. Results and discussion

4.1. Roles of physical properties

Before discussing the obtained results, we briefly introduce the basic equations and relevant quantities for droplet vaporization (a detailed treatment is given e.g. by Law [34]). The vaporization is governed by transport of heat and mass to and from the droplet, which is quantified by the transfer numbers for heat, B_T, and for mass, B_M, respectively. These depend on the fuel mass fraction Y_s and temperature T_s at the droplet surface, heat of vaporization H_v, specific heat C_p and ambient gas temperature T_∞ according to

$$B_\mathrm{M} = \frac{Y_\mathrm{s}}{1 - Y_\mathrm{s}} \quad \text{and} \quad B_\mathrm{T} = \frac{C_\mathrm{p}(T_\infty - T_\mathrm{s})}{H_\mathrm{v}}. \tag{1}$$

For a given T_∞, Y_s and T_s are calculated using the equations of state and for fuel vapor pressure (not stated here). Under steady-state conditions, $B_\mathrm{T} = B_\mathrm{M} \equiv B$ and the squared droplet diameter decreases linearly with time as $D^2(t) = D_0^2 - Kt$. The vaporization rate $K = -\partial D^2/\partial t$ is then given by

$$K = \frac{8\rho_g \mathcal{D}}{\rho_l} \ln(1 + B), \tag{2}$$

where ρ_g and ρ_l denote the densities of gas and liquid, respectively, and $\mathcal{D}$ is the diffusion coefficient of fuel vapor.

At a given T_∞, B depends mainly on the fuel boiling temperature T_b, which influences Y_s and T_s, and H_v. If,

Name	Type	Boiling range [°C]			H_v at 150°C [kJ / l]	Aromatic content [Vol.%]	References
		T_0	T_{50}	T_{100}			
Jet A, POSF 10325	CJF	159	205	271	205	17.0	[6, 9, 20, 33]
JP-5, POSF 10289	CJF	178	220	260	208	18.0	[6, 9, 20, 33]
JP-8, POSF 10264	CJF	150	190	257	196	11.2	[6, 33]
HEFA	AJF	144	202	256	191	<0.5	[3]
AtJ	AJF	170	181	259	n/a	<0.2	[3, 6, 9, 33]
Farnesane	AJF	247			n/a	0	[3]
n-Nonane	SC	151			176	0	[25]
n-Dodecane	SC	216			188	0	[9, 25]
n-Pentadecane	SC	271			n/a	0	[25]

Table 1: Boiling points / ranges, heat of vaporization and aromatic content of tested fuels. The values of H_v are obtained from various sources included in the DLR Spraysim model. References to more detailed specifications or other studies of vaporization behavior are provided.

however, $T_\infty \gg T_b$ (say, $T_\infty - T_b > 500$ K), $T_s \approx T_b$ and thus $B \approx C_p(T_\infty - T_b)/H_v$. The vaporization rate K then only depends slightly on T_b and largely on H_v.

To further elucidate the temperature dependence of K, a comparison of the vaporization of n-dodecane and 1-hexanol using the present experiment is shown in Fig. 4a. 1-hexanol is not considered for jet fuels, but was chosen because it exhibits a markedly higher H_v of 603 J/g (at 25°C) than n-dodecane with 361 J/g, while the latter has a significantly higher T_b of 216°C compared to 157°C for 1-hexanol. After an initial period where D remains constant, D first increases due to thermal expansion caused by the increase of ambient temperature (cf. Fig. 2). The subsequent decrease of D due to vaporization then starts notably later for n-dodecane due to its considerably higher T_b. For $t/D_0^2 \gtrsim 3$ s/mm^2, however, it is seen that n-dodecane vaporizes remarkably faster than 1-hexanol due to its lower H_v and eventually finishes vaporization earlier. This demonstrates that for high-temperature vaporization typical of technical combustors, not only distillation curves are relevant but also the values of H_v. In Table 1, values of H_v are provided (as far as available) for T=150°C, which roughly represents the liquid droplet temperature during vaporization.

4.2. Conventional jet fuels

In Fig. 4b, the droplet vaporization is shown for the 3 CJFs. After the initial phase of thermal expansion, it is seen that vaporization starts first for JP-8 followed by Jet A and then JP-5. This coincides well with the shifts of the respective boiling curves plotted in Fig. 3. For $t/D_0^2 \gtrsim 3$ s/mm^2, by contrast, no further relative deviations between the fuels are observed. This is in accordance with the conclusions made in Sect. 4.1 that the influence of T_b is highest at relatively low T_∞ and decreases at higher T_∞.

4.3. Alternative jet fuels

The vaporization of AJFs is compared to Jet A in Fig. 4c. The evolution of HEFA is very similar to Jet A, except for a slightly faster vaporization during the initial phase shown in the zoomed inset. This agrees with the presence of more volatile light-end components in HEFA (cf. Fig. 3). AtJ and Farnesane, by contrast, vaporize significantly earlier and later, respectively, than Jet A in accordance with their differences in boiling temperatures. Thereby they lie outside the range of the CJFs shown in Fig. 4b. It is noted, however, that their blending ratios are restricted to a maximum of 50% and 10%, respectively [4].

4.4. Single-component fuels

In Fig. 4d, the vaporization of Jet A is compared to 3 n-alkanes whose values of T_b lie near T_0, T_{50} and T_{100}, respectively, of Jet A. It is seen that n-dodecane with $T_b \approx T_{50}$ behaves roughly similar to Jet A. During the initial phase shown in the zoomed inset, however, Jet A vaporizes considerably faster. This indicates the preferential vaporization of light-end components of Jet A during this phase. For $t/D_0^2 > 4$ s/mm^2, by contrast, the vaporization rate of n-dodecane is higher than that of Jet A. This agrees with the higher T_b of the remaining heavy-end components of Jet A and its higher H_v due to the content of aromatics (cf. Table 1). Comparing the 3 n-alkanes, it is seen that their vaporization rates diverge during the initial phase (zoomed inset) at relatively low temperature where the influence of T_b is largest, whereas their evolutions of $D(t)$ are similar for the higher temperatures during the later phase. Like for

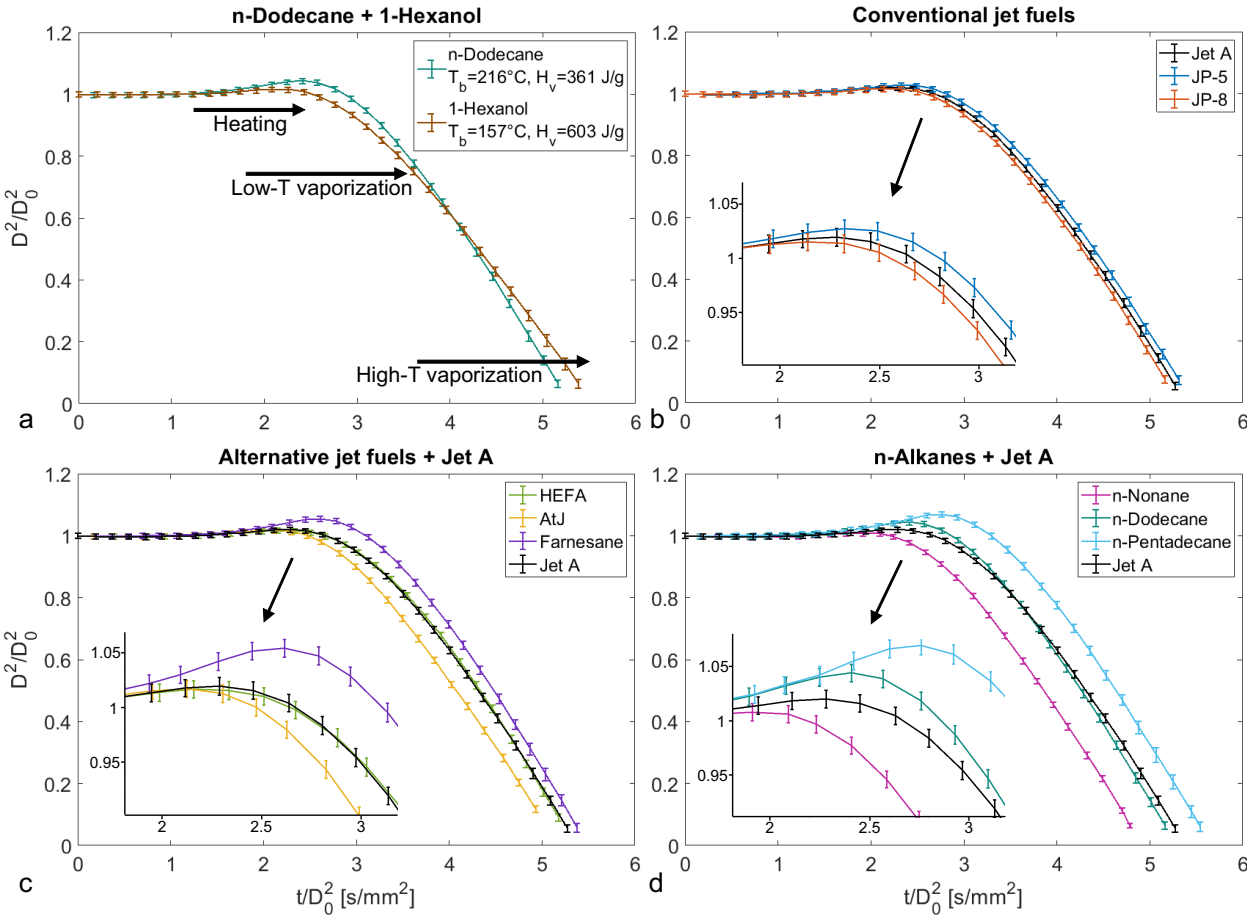

Figure 4: Experimental results for temporal evolution of squared droplet diameter D^2 for the fuels tested in this study. Both D^2 and t are normalized by the squared initial diameter D_0^2. The line colors correspond to those of the respective distillation curves in Fig. 3.

the CJFs reported in Sect. 4.2, this agrees with the discussion of the role of T_b in Sect. 4.1.

4.5. Numerical simulation

Figure 5 compares the measurements for the 3 CJFs to the results of the numerical modeling using the multi-component CTM described in Sect. 2.2. In general the simulation predicts very well the evolutions of $D(t)$ plotted in Fig. 5a. The fuel-dependent differences of the evolutions of $D(t)$ in the earlier phase (zoomed inset) are well captured, whereas the absolute values of D are somewhat higher.

The plots of vaporization rate $K(x)$ in Fig. 5b show that K first decreases due to thermal expansion until $x \approx 12$ mm, and then continuously increases due to the rise of $T_\infty(x)$ (cf. Fig. 2). It is seen that generally K is highest for JP-8 followed by Jet A and JP-5 in accordance with the respective order of boiling temperatures and values of H_v. The slight underpredictions of K correspond to the overpredictions of D in Fig. 5a.

One possible cause of the remaining deviations from experiment might be the use of the RMA for droplet modeling according to Sect. 2.2. For the high rates of vaporization at the present conditions, the droplet internal mixing cannot be considered as infinitely fast, and thus the RMA is not strictly valid. On the other hand, the RMA substantially reduces computational cost compared to very expensive modeling of multi-component internal transport, which is important for engineering applications. Apart from the RMA, the deviations might also be due to errors in the computed velocities and temperatures of gas in the channel or due to effects of radiation, which are not included in the model. A more detailed assessment of the deviations, however, is beyond the scope of this study and subject of future work. In total, the overall good predictions of the numerical model

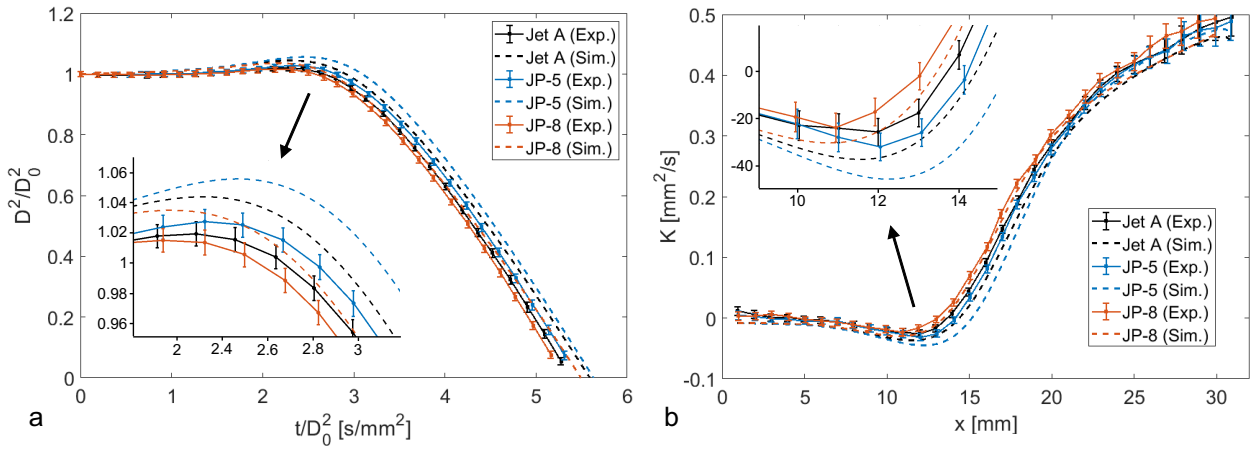

Figure 5: Comparisons of measurement and simulation for CJFs: (a) normalized squared droplet diameter and (b) vaporization rate K.

make it suitable for most engineering purposes.

5. Conclusions

The present work was motivated by a lack of suitable validation data for models of multi-component droplet vaporization for aviation-relevant fuels at realistic conditions. Such validation requires well-defined boundary conditions of the ambient gaseous flow and the exact fuel composition. The present article describes a newly designed experiment for studying vaporization of multi-component fuel droplets of realistic size, which provides precise measurements of droplet diameter over time under well-defined conditions with temperatures similar to technical combustors. Measurements for various well-specified conventional and alternative jet fuels showed that the differences of their vaporization can be accurately resolved and related to physical properties. A comparison of the time-series of squared droplet diameter for pure n-dodecane and a multi-component Jet A further revealed that the latter exhibits a significant degree of preferential vaporization. The results were then used for assessment of a multi-component vaporization model that has been employed before in a recent LES of an aero-engine combustor [11]. The comparisons demonstrated that the present model generally provides accurate prediction of droplet vaporization including fuel-dependent effects, with a slight fuel-indepedent overprediction of droplet diameters. The latter may be a starting point for further model improvement as a subject of future work.

Acknowledgments

Funding from the EU within the project JETSCREEN (agreement No. 723525) is gratefully acknowledged. We thank T. Edwards and M. Colket from the US NJFCP for providing the fuels Jet A, JP-5 and JP-8, and colleagues of DLR VT-CHA for help with fuel preparation.

References

[1] D. Lee, G. Pitari, V. Grewe, K. Gierens, J. Penner, et al., Transport impacts on atmosphere and climate: Aviation, Atmos. Environ. 44 (2010) 4678–4734.

[2] S. Blakey, L. Rye, C. W. Wilson, Aviation gas turbine alternative fuels: A review, Proc. Combust. Inst. 33 (2011) 2863–2885.

[3] M. Kaltschmitt, U. Neuling (Eds.), Biokerosene - Status and Prospects, Springer, 2018.

[4] ASTM D7566, Standard Specification for Aviation Turbine Fuel Containing Synthesized Hydrocarbons, ASTM International, West Conshohocken, USA (2018).

[5] https://www.jetscreen-h2020.eu/.

[6] M. Colket, J. Heyne, M. Rumizen, M. Gupta, T. Edwards, et al., Overview of the national jet fuels combustion program, AIAA J. 55 (2017) 1087–1104.

[7] T. Edwards, C. Moses, F. Dryer, Evaluation of combustion performance of alternative aviation fuels, 46th AIAA/ASME/SAE/ASEE Joint Propulsion Conference, AIAA 2010-7155, 2010.

[8] L. Esclapez, P. C. Ma, E. Mayhew, R. Xu, S. Stouffer, et al., Fuel effects on lean blow-out in a realistic gas turbine combustor, Combust. Flame 181 (2017) 82–99.

[9] S. H. Won, N. Rock, S. J. Lim, S. Nates, D. Carpenter, et al., Preferential vaporization impacts on lean blow-out of liquid fueled combustors, Combust. Flame 205 (2019) 295–304.

[10] B. Abramzon, W. Sirignano, Droplet vaporization model for spray combustion calculations, Int. J. Heat Mass Transf. 32 (9) (1989) 1605–1618.

[11] G. Eckel, J. Grohmann, L. Cantu, N. Slavinskaya, T. Kathrotia, M. Rachner, P. Le Clercq, W. Meier, M. Aigner, LES of

a swirl-stabilized kerosene spray flame with a multi-component vaporization model and detailed chemistry, Combust. Flame 207 (2019) 134–152.

[12] A. Stagni, L. Esclapez, P. Govindaraju, A. Cuoci, T. Faravelli, M. Ihme, The role of preferential evaporation on the ignition of multicomponent fuels in a homogeneous spray/air mixture, Proc. Combust. Inst. 36 (2017) 2483–2491.

[13] J. Tamim, W. L. Hallett, A continuous thermodynamics model for multicomponent droplet vaporization, Chem. Eng. Sci. 50 (18) (1995) 2933–2942.

[14] P. Le Clercq, J. Bellan, Direct numerical simulation of gaseous mixing layers laden with multicomponent-liquid drops: liquid-specific effects, J. Fluid Mech. 533 (2005) 1087–1104.

[15] P. Le Clercq, N. Doue, M. Rachner, M. Aigner, Validation of a multicomponent-fuel model for spray computations, 47th AIAA Aerospace Sciences Meeting, AIAA 2009-1188, 2009.

[16] A. Y. Cooney, S. L. Singer, Modeling multicomponent fuel droplet vaporization with finite liquid diffusivity using coupled algebraic-DQMoM with delumping, Fuel 212 (2018) 554–565.

[17] M. Burger, R. Schmehl, K. Prommersberger, O. Schäfer, R. Koch, S. Wittig, Droplet evaporation modeling by the distillation curve model: accounting for kerosene fuel and elevated pressures, Int. J. Heat Mass Transf. 46 (2003) 4403–4412.

[18] Y. Ra, R. D. Reitz, A vaporization model for discrete multi-component fuel sprays, Int. J. Multiph. Flow 35 (2009) 101–117.

[19] S. Sazhin, A. Elwardany, E. Sazhina, M. Heikal, A quasi-discrete model for heating and evaporation of complex multi-component hydrocarbon fuel droplets, Int. J. Heat Mass Transf. 54 (2011) 4325–4332.

[20] P. B. Govindaraju, M. Ihme, Group contribution method for multicomponent evaporation with application to transportation fuels, Int. J. Heat Mass Transf. 102 (2016) 833–845.

[21] I. Gökalp, C. Chauveau, H. Berrekam, N. Ramos-Arroyo, Vaporization of miscible binary fuel droplets under laminar and turbulent convective conditions, Atomization Spray. 8 (1994) 661–676.

[22] H. Nomura, Y. Ujiie, H. Rath, J. Sato, M. Kono, Experimental study on highpressure droplet evaporation using microgravity conditions, Symp. (Int.) Combust. 26 (1996) 1267–1273.

[23] T. Runge, M. Teske, Low-temperature vaporization of JP-4 and JP-8 fuel droplets, Atomization Spray. 8 (1988) 25–40.

[24] M. Ochs, J. Gass, L. Reh, Convective vaporization of freely moving fuel droplets in a hot air flow, ILASS-Europe, Zürich, Switzerland, 2001.

[25] J. Wilms, Evaporation of multicomponent droplets, Ph.D. thesis, University of Stuttgart (2005).

[26] A. Muelas, P. Remacha, J. Ballester, Droplet combustion and sooting characteristics of UCO biodiesel, heating oil and their mixtures under realistic conditions, Combust. Flame 203 (2019) 190–203.

[27] D. Honnery, D. Nguyen, J. Soria, Microdroplet evaporation under increasing temperature conditions: Experiments and modelling, Fuel 105 (2013) 247–257.

[28] P. Weigand, R. Lückerath, W. Meier, Documentation of flat premixed laminar CH_4/air standard flames: temperatures and species concentrations, Institute of Combustion Technology, German Aerospace Center (DLR).

[29] C. Morley, Gaseq v0.79, http://www.gaseq.co.uk (2005).

[30] M. Di Domenico, P. Gerlinger, B. Noll, Numerical simulations of confined, turbulent, lean, premixed flames using a detailed chemistry combustion model, ASME Turbo Expo, GT2011-45520, 2011.

[31] T. Blacha, M. Di Domenico, M. Köhler, P. Gerlinger, M. Aigner, Soot modeling in a turbulent unconfined C_2H_4/air jet flame, 49th AIAA aerospace sciences meeting including the new horizons forum and aerospace exposition, 2011.

[32] G. Eckel, P. Le Clercq, T. Kathrotia, A. Saenger, S. Fleck, M. Mancini, T. Kolb, M. Aigner, Entrained flow gasification. Part 3: Insight into the injector near-field by large eddy simulation with detailed chemistry, Fuel 223 (2018) 164–178.

[33] T. Edwards, Reference jet fuels for combustion testing, 55th AIAA Aerospace Sciences Meeting, AIAA 2017-0146, 2017.

[34] C. Law, Recent advances in droplet vaporization and combustion, Prog. Energy. Combust. Sci. 8 (1982) 171–201.